Fermi National Accelerator Laboratory and University of Milan

Summer Internship Program

Transverse Momentum Distributions for Vector Boson production at the Tevatron

Supervisor: Prof. Ashutosh V. Kotwal

Student: Fabrizio Cimaglia

Final Report - Batavia - September 22 2015

Contents

Abstract

We present a study of tranverse-momentum distributions for vector boson production at the Tevatron energies. The analysis is performed with the software `DYqT` and `DYRes` that compute Quantum-Cromo Dynamics (QCD) corrections respectively up to NLO+NNLL and NNLO+NNLL. The computation encodes vector boson spin correlations, finite-width effects and a full dependence on the final-state lepton(s) kinematics. We report a brief description of the resummation approach involved in the computation and focus on the variation of the renormalization, factorization and resummation scales. We finally compare results obtained with the following PDFs sets: `MSTW2008`, `MSTW2004`, `NNPDF3.0` and `NNPDF2.3`.

1 Introduction

The production of vector bosons at hadron colliders provides an important test for the Standard Model (SM). It allows accurate calculations of fundamental parameters along with specific constraints on new physics. It is thus a leading goal to reach strict theoretical predictions for Drell-Yan (DY) mechanism [7] which is a benchmark for studying collider physics. This requires the evaluation of QCD corrections, which can be perturbatively computed as series of exponential in the strong coupling constant α_s. QCD corrections have achieved the next-to-next-to-leading order (NNLO) in perturbation theory for the computation of the total cross section of vector boson decays as well as rapidity distributions in [8, 9, 10, 22, 12]. Electroweak radiative corrections (EW) are also available for both W and Z/γ^*.

A staple observable is the transverse-momentum (p_T) distribution of vector boson. It is essential in order to obtain an accurate measurement of W boson mass (M_W). QCD corrections are known at $\mathcal{O}(\alpha_s^2)$ order in the region of large p_T ($p_T \approx m_V$). Recently the computation for vector boson production in addition of a jet has performed in [13, 14] at the order $\mathcal{O}(\alpha_s^3)$. In the region where $p_T \approx m_V$, m_V being the mass of the vector boson, the QCD perturbative series is controlled by a small expansion parameter, $\alpha_s(m_V)$, and fixed-order calculations are theoretically justified. In this region, the QCD radiative corrections are known up to NNLO. In the small p_T region ($p_T \ll m_V$), the convergence of the fixed-order expansion is spoiled, since the coefficients of the perturbative series are enhanced by powers of large logarithmic terms, $\alpha_s^n \ln^m(m_V^2/p_T^2)$, where $1 \leq m \leq 2n-1$. To obtain reliable predictions, these terms have to be resummed to all perturbative orders.

The method to systematically perform all-order resummation of classes of logarithmically-enhanced terms at small p_T is known [15, 16, 17]. The resummed and fixed-order procedures at small and large values of p_T can then be matched at intermediate values of p_T , to obtain QCD predictions for the entire range of transverse momenta. Studies of the vector boson p_T distribution have been performed by combining resummed and fixed-order perturbation theory at various levels of accuracy . A first method to perform resummation has been discussed in [18]. The resummed distribution is factorized in terms of a universal transverse-momentum form factor and a single process-dependent hard function. In the small-p_T region, the logarithmic terms of the form factor are systematically resummed in exponential form. A constraint of perturbative unitarity is imposed on the resummed terms, to the purpose of reducing the effect of unjustified higher-order contributions at large values of p_T and, especially, at intermediate values of p_T .The resummed and fixed-order calculations, which are valid at small and large values of p_T , respectively, can be consistently matched at intermediate values of p_T to achieve a uniform theoretical accuracy for the entire range of transverse momenta.

Hadron colliders experiments can directly measure only the decay products of vector bosons in one finite kinematical region. Therefore, it is important to include the vector boson leptonic decay in the theoretical calculations, by retaining the kinematics of the final-state leptons. In this way it is possible to obtain predictions for the transverse-momentum distribution of the measured leptons. This is specially relevant in the case of W production where, because of the final-state neutrino, the transverse momentum of the vector boson can only be reconstructed through a measure of the hadronic recoil. Moreover, in both cases of W and Z production, the inclusion of the leptonic decay allows applying kinematical selection cuts, thus providing a more realistic simulation of the actual experimental analysis. The method we use combines resummation at the next-to-next-to-leading logarithmic (NNLL) accuracy in the small-p_T region with the fixed-order results at $\mathcal{O}(\alpha_s^2)$ in the large-p_T region. This leads to a calculation with uniform theoretical accuracy from small to intermediate values of p_T. Moreover, at large values of p_T the calculation implements a unitarity constraint that guarantees to exactly reproduce the NNLO value of the total cross section after integration over p_T .

The programs used for p_T spectrum production are `DYRes` and `DYqT`. These High-Energy QCD softwares allow respectively NNLL+NNLO and NLO+NNLL calculations including leptonic decay of the vector boson with the corresponding spin correlations. The spin of the vector boson dynamically correlates the decaying lepton momenta with the transverse momentum acquired by the vector boson through its production mechanism. Therefore, the inclusion of the full dependence on the lepton decay variables in the resummed calculation requires a theoretical discussion on the treatment of the p_T

recoil due to the transverse momentum of the vector boson. DYRes treats the p_T recoil by introducing a general procedure that is directly applicable to p_T resummed calculations for generic production processes of high-mass systems in hadron collisions.

This work is organized as follows: we discuss W along with Z p_T spectra using the resummation method of DYRes firstly performed in [19] for the LHC. We present the theoretical approach for vector boson resummation introduced in [20], discuss some physical constraints at CDF in order to introduce our phenomenological approach. Finally, we present quantitative results.

1.1 W boson production and decay at the Tevatron

The analysis we present is oriented to a precise measurement of W boson mass (M_W) with the Collider Detector at Fermilab (CDF). It is known that the spontaneous symmetry-breaking, which is in the Standard Model (SM) the Higgs mechanism, states that M_W in the *on-shell* scheme can be estimated as follows

$$M_W^2 = \frac{\hbar^3\pi}{c}\frac{\alpha_{EM}}{\sqrt{2}G_F(1-M_W^2/M_Z^2)(1+\Delta r)} \tag{1}$$

where α_{EM} is the electromagnetic coupling at $Q = M_Z c^2$, G_F is the Fermi weak coupling extracted from the muon lifetime measurement, M_Z is the Z-boson mass, and $\Delta r = 3.58\%$ includes all radiative corrections. In the SM, the electroweak radiative corrections are dominated by loops containing top and bottom quarks, but also depend logarithmically on the mass of the Higgs boson M_H through loops containing the Higgs boson. Loops in the W boson propagator contribute to the correction Δr, defined in the following expression for the W -boson mass M_W in the on-shell scheme [1].

Following the discovery of the W boson in 1983 at the UA1and UA2 experiments [2], measurements of M_W have been performed with increasing precision using $\sqrt{s} = 1.8$ TeV $p\overline{p}$ collision at the CDF [3] and D0 [4] experiments (RUN 1). The CDF [5] and D0 [6] (Run 2) at $\sqrt{s} = 1.96$ TeV have produced the combined world measurement to $M_W = 80385 \pm 15$ MeV/c^2. The measurement $M_W = 80385 \pm 19$ MeV/c^2 at the CDF is considered as the world best value to date.

1.1.1 M_W measurement at the Tevatron

In $p\overline{p}$ collisions at $\sqrt{s} = 1.96$, W bosons are primarily produced via s-channel annihilation of valence quarks with a smaller contribution from sea-quark annihilation. These initial-state quarks radiate gluons that can produce hadronic jets in the detector. The W boson decays either to a quark-antiquark pair ($q\overline{q}'$) or to a charged lepton and neutrino ($l\nu$). The hadronic decays are overwhelmed by background at the Tevatron due to the high rate of quark and gluon production through QCD interactions. Decays to τ leptons are not included since the momentum measurement of a τ lepton is not as precise as that of an electron or muon. The mass of the W boson is therefore measured using the decays $W^{\pm} \to l^{\pm}\nu_l$, $(l = e, \mu)$, which have about 22% total branching fraction. Samples selected with the corresponding Z-boson decays, $Z^0 \to l^+l^-$, are used for calibration.
The CDF experiment uses a right-handed coordinate system in which the z axis is centered at the middle of the detector and points along a tangent to the Tevatron ring in the proton-beam direction. The remaining Cartesian coordinates are defined with $+x$ pointing outward and $+y$ upward from the Tevatron ring, respectively. Transverse quantities such as transverse momentum are projections onto the (x, y) plane. The interacting protons and antiprotons have negligible net transverse momentum. Electron energy measured in the calorimeter is denoted as E and the corresponding transverse momentum E_T is derived using the direction of the reconstructed particle trajectory (track) and neglecting the electron mass. For transverse-momentum conservation , the transverse-momentum of the neutrino p_T^{ν} in W leptonic decay is evaluated as $p_T^{\nu} = -p_T^l - u_T$, where p_T^l is the transverse-momentum of the charged lepton and u_T the recoil - defined as the negative of the transverse-momentum of the vector boson.

1.1.2 Measurement strategy at CDF

The measurement is performed by fitting for M_W using three transverse quantities that do not depend on the unmeasured longitudinal neutrino momentum: p_T^l, p_T^ν , and the transverse-mass

$$m_T = \sqrt{2p_T^l p_T^\nu (1 - \cos\Delta\phi)} \tag{2}$$

where $\Delta\phi$ is the angle between the neutrino and charged lepton momenta in the transverse plane. Candidate events are selected with $u_T \ll p_T^l$, so the neutrino momentum can be approximated as $p_T^\nu \approx p_T^l + u_{||}$ and the transverse mass can be approximated as $m_T \approx 2p_T^l + u_{||}$. These relations demonstrate the importance of modeling $u_{||}$ accurately relative to other recoil components. They also demonstrate that the three fit variables have varying degrees of sensitivity to the modeling of the recoil and the p_T of the W boson. High precision determination of p_T^l is crucial to this measurement: a given fractional uncertainty on p_T^l translates into an equivalent fractional uncertainty on M_W. The absolute scale of the calibrated track momentum is tested by measuring the Z-boson mass in $Z^0 \to \mu^+\mu^-$ decays and comparing it to the known value. After including the M_Z measurement, the calibration is applied to the measurement of M_W in $W^\pm \to \mu^\pm\nu_\mu$ decays and in the procedure used for the calibration of the electron energy scale in the calorimeter. Since W and Z bosons are produced from a similar initial state at a similar energy scale, the hadronic recoil is similar in the two processes. To model the detector response to this recoil, a heuristic description of the contributing processes is developed and the model parameters are tuned using fully-reconstructed $Z^0 \to \mu^+\mu^-$ data. The inclusive p_T distribution of produced W bosons is also tuned using $Z^0 \to \mu^+\mu^-$ data by combining the measured p_T distribution of Z bosons with a precise calculation of the relative p_T distributions of W and Z bosons. As with the fits for M_Z , a single blinding offset in the range $[-75, 75]$ MeV is applied to all M_W fits for the course of the analysis. This offset differs from that applied to the M_Z fits. No changes are made to the analysis once the offsets to the M_W fit results are removed.

2 Trensverse-momentum Resummation

This section is devoted to a brief recall of resummation formalism applied to the production of vector boson. The formalism we expose is implemented in both `DYRes` and `DYqT`.

2.1 Resummation formalism for Vector-Boson Production

The bulk of the vector boson cross section is produced in the small-p_T region, where the reliability of the fixed-order expansion is spoiled by the presence of large logarithmic corrections of soft and collinear origin. To obtain reliable predictions, these logarithmically-enhanced terms have to be evaluated and systematically resummed to all orders in perturbation theory . In recent years, the resummation of small- p_T logarithms has been reformulated by using Soft Collinear Effective Theory (SCET) methods and transverse-momentum dependent (TMD) factorization.

Let us consider the inclusive hard-scattering process

$$h_1(p_1) + h_2(p_2) \longrightarrow F(M, p_T) + X, \tag{3}$$

where h_1 and h_2 forms the hadronic initial state with momenta p_1 and p_2, $F(M, p_T)$ is a detected final state and X is arbitrary. The observed final state F is a generic system of non-QCD partons such as one or more vector bosons. We do not consider the production of strongly interacting particles (hadrons, jets, heavy quarks, ...), since in this case the resummation formalism of small-p_T logarithms has not yet been fully developed.

According to the QCD factorization theorem the corresponding transverse- momentum differential cross section $d\hat{\sigma}_F/dp_T^2$ can be written as

$$\frac{d\hat{\sigma}_F}{dp_T^2}(p_T, M, s) = \sum_{a,b} \int_0^1 dx_1 \int_0^1 dx_2 f_{a/h_1}(x_1, \mu_F^2) f_{a/h_2}(x_2, \mu_F^2) \frac{d\hat{\sigma}_{Fab}}{dp_T^2} \left((p_T, m_V, \hat{s}, \alpha_s(\mu_R^2), \mu_R^2, \mu_F^2)\right), \tag{4}$$

where $f_{a/h_1}(x_1, \mu_F^2)$ and $f_{a/h_2}(x_2, \mu_F^2)$ are the parton densities of the colliding hadrons, μ_F and μ_R respectively the factorization and renormalization scales, $d\hat{\sigma}_{Fab}/dp_T^2$ the partonic cross section, s the center-of-mass energy, $\hat{s} = x_1 x_2 s$ the partonic center-of-mass energy. The partonic cross section is computable in QCD perturbation theory as a power series expansion in α_S. We assume that at the parton level the system F is produced so that the corresponding cross section is $d\hat{\sigma}_F/dp_T^2(0) \approx \delta(p_T^2)$ at the lower order.

As evinced by the perturbation theory, the higher-order perturbative contributions to the partonic cross section $d\hat{\sigma}_{Fab}/dp_T^2$ contain logarithmic terms of the type $\ln^m(m_V^2/p_T^2)$ that become large in the small-p_T region. Therefore, we introduce the following decomposition of the partonic cross section in the Eq. 4

$$\frac{d\hat{\sigma}_{Fab}}{dp_T^2} = \frac{d\hat{\sigma}_{Fab}^{(\text{res.})}}{dp_T^2} + \frac{d\hat{\sigma}_{Fab}^{(\text{fin.})}}{dp_T^2}, \tag{5}$$

where the logarithmical terms are contained in $d\hat{\sigma}_{Fab}^{(res.)}$. at small p_T , and has to be evaluated by resumming them to all orders in α_S. The second term $d\hat{\sigma}_{Fab}^{(fin.)}$ is free of these contributions, thus can be computed through a matrix element approach. To be precise, we define the so-called "finite" part of the total cross section as follows

$$\lim_{P_T \to 0} \int_0^{P_T^2} dp_T^2 \left[\frac{d\hat{\sigma}_{Fab}^{(\text{fin.})}}{dp_T^2},\right]_{\text{f.o.}} = 0, \tag{6}$$

where the right-hand side tends to zero order-by-order in perturbation theory.

In summary, the p_T distribution in Eq. 4 is evaluated, in practice, by replacing the partonic cross section on the right-hand side as follows

$$\frac{d\hat{\sigma}_{Fab}}{dp_T^2} \longrightarrow \left[\frac{d\hat{\sigma}_{Fab}^{(\text{res.})}}{dp_T^2}\right]_{\text{l.a.}} + \left[\frac{d\hat{\sigma}_{Fab}^{(\text{fin.})}}{dp_T^2}\right]_{\text{f.o.}}, \tag{7}$$

where we compute the truncation at a given order in perturbation theory. Note that the "res." part becomes relevant at low-pT, whereas the fixed-order component dominates at large-p_T. One of the aim of this review is to present how these two sides are involved in the computation and affect the total cross section. The software `DYRes` allows the computation of fixed-order as well as resummed part separately, then they are combined. The two components have to be consistently matched in order to obtain a suitable theoretical accuracy all over the range of p_T.

This matching procedure guarantees that the replacement in Eq. 7 retains the full information of the perturbative calculation up to the specified fixed order plus resummation of logarithmically- enhanced contributions from higher orders. The matching guarantees the replacement is perturbatively coherent[1].Thus, the small-p_T along with large-p_T are combined without double counting.

The resummed contributions that are present in the term of Eq. 7 are necessary and fully justified at small-p_T . Nonetheless they can lead to sizable higher-order perturbative effects also at large-p_T , where the small-p_T logarithmic approximation is not valid. To reduce the impact of these unjustified higher-order terms, we require that they give no contributions to the most basic quantity, namely the total cross section, that is not affected by small-p_T logarithmic terms. We thus impose that the integral over p_T of Eq. 7 exactly reproduces the fixed-order calculation of the total cross section. Since $d\hat{\sigma}^{(\text{fin.})}$ is evaluated in fixed-order perturbation theory, the perturbative constraint on the total cross section is achieved by imposing the following condition

$$\int_0^\infty dp_T^2 \left[\frac{d\hat{\sigma}_{Fab}^{(\text{res.})}}{dp_T^2}\right]_{\text{l.a.}} = \int_0^\infty dp_T^2 \left[\frac{d\hat{\sigma}_{Fab}^{(\text{res.})}}{dp_T^2}\right]_{\text{f.o.}} \tag{8}$$

Since resummed and fixed-order perturbation theory controls the small-p_T and large-p_T regions respectively, the total cross section constraint mainly acts on the size of the higher-order contributions introduced in the intermediate-p_T region by the matching procedure.

A distinctive feature of the formalism illustrated as far is that we implement perturbative QCD resummation at the level of the partonic cross section. In the factorization formula 4, the parton densities are thus evaluated at the factorization scale μ_F , as in the customary perturbative calculations at large p_T . Although we are dealing with a process characterized by two distinct hard scales, p_T and m_V, the dominant effects from the scale region $p_T \ll m_V$ are explicitly taken into account through all-order resummation. Therefore, the central value of μ_F and μ_R has to be set equal to m_V, the 'remaining' typical hard scale of the process. Then the theoretical accuracy of the resummed calculation can be investigated as in customary fixed-order calculations, by varying μ_F and μ_R around this central value.

2.1.1 The resummed component at NNLL

In this section we specialize the resummed component in Eq. 7 at the NNLL. The resummation procedure has to be carried out in the impact- parameter space, to correctly take into account the kinematics constraint of transverse-momentum conservation. A fully exhaustive deduction of the argument has been performed in [20]. In this review we report the main result at NNLL which is stated as follows: the resummed component of the transverse-momentum cross section is obtained by

[1] the fixed-order truncation of the right-hand side of Eq. 5 exactly reproduces the customary fixed-order truncation of the partonic cross section in Eq. 4.

performing the inverse Fourier (Bessel) transformation with respect to the impact parameter b by the following formula

$$\frac{d\hat{\sigma}^{(\mathrm{res.})}_{Fab}}{dp_T^2}\left(p_T, m_V, \hat{s}, \alpha_s(\mu_R^2), \mu_R^2, \mu_F^2\right) = \frac{m_V^2}{\hat{s}} \int \frac{d^2\mathbf{b}}{4\pi} e^{i\mathbf{b}p_T} \mathcal{W}^F_{ab}\left(\mathbf{b}, m_V, \hat{s}, \alpha_s(\mu_R^2), \mu_R^2, \mu_F^2\right) \tag{9}$$

The perturbative and process-dependent factor $\mathcal{W}^F$ involves the all-order dependence on the large logarithms $\ln m_V^2 b^2$ at large b, which correspond to the p_T-space terms $\ln m_V^2/p_T$ that are logarithmically enhanced at small p_T. The resummation of $\mathcal{W}^F$ is computed as exponential series of a function $\mathcal{G}$ depending from μ_R, μ_F and the so-called resummation scale Q. Variations of these scales could be used to estimate theoretical uncertainties for logarithmic corrections. Usually, $\mathcal{G}$ is expressed as follows

$$\mathcal{G}_N\left(\alpha_S, L, m_V^2/\mu_R, m_V^2/Q^2\right) = \sum_{n=4}^{\infty} \left(\frac{\alpha_S}{\pi}\right)^{n-2} g_N^{(n)}\left(\alpha_S L, m_V^2/\mu_R^2, m_V^2/Q^2\right) \tag{10}$$

where, defining the parameter b_0 conventionally, L is stated as follows

$$L \doteq \ln\left(\frac{b^2Q^2}{b_0^2}\right) \tag{11}$$

Thus, the resummation at NNLL is stated in terms of a specific computation of g_N at a given order in perturbation theory. The NNLL contribution is given evaluating $g_N^{(3)}$ as follows

$$\begin{aligned} g_N^{(3)}\left(\alpha_S L, \frac{m_V^2}{\mu_R^2}, \frac{m_V^2}{Q^2}\right) = &-\frac{A^{(3)}}{2\beta_0^2}\frac{\lambda^2}{(1-\lambda)^2} - \frac{\overline{B}_N^{(2)}}{\beta_0}\frac{\lambda}{1-\lambda} + \frac{A^{(2)}\beta_1}{\beta_0}\left(\frac{\lambda}{2}\frac{(3\lambda-2)}{2(1-\lambda)^2} - \frac{(1-2\lambda)\ln(1-\lambda))}{(1-\lambda)^2}\right) + \\ &+\frac{\overline{B}_N^{(1)}\beta_1}{\beta_0^2}\left(\frac{\lambda}{1-\lambda} + \frac{\ln(1-\lambda)}{1-\lambda}\right) - \frac{A^{(1)}}{2}\frac{\lambda^2}{(1-\lambda)^2}\ln^2\frac{Q^2}{\mu_R^2} + \\ &+\ln\frac{Q^2}{\mu_R^2}\left(B_N^{(1)}\frac{\lambda}{1-\lambda} + \frac{A^{(2)}}{\beta_0}\frac{\lambda^2}{(1-\lambda)^2} + A^{(1)}\frac{\beta_1}{\beta_0}\left(\frac{\lambda}{1-\lambda} + \frac{1+2\lambda}{(1-\lambda)^2}\ln(1-\lambda)\right)\right) + \\ &+A^{(1)}\left(\frac{\beta_1^2}{2\beta_0^2}\frac{1-2\lambda}{(1-\lambda)^2}\ln^2(1-\lambda) + \ln(1-\lambda)\left[\frac{\beta_0\beta_2-\beta_1^2}{\beta_0^4} + \frac{\beta_1^2}{\beta_0^4(1-\lambda)} + \left(\beta_0\beta_2(2-3\lambda)+\beta_1^2\lambda\right)\right]\right) \end{aligned} \tag{12}$$

where we define the following parameters

$$\lambda = \frac{1}{\pi}\beta_0\alpha_S(\mu_R^2)L, \tag{13}$$

$$\overline{B}_N^{(n)} = \tilde{B}_N^{(n)} + A^{(n)}\ln\frac{m_V^2}{Q^2}, \tag{14}$$

and the β_n functions are the coefficients of the following expansion

$$\frac{d\ln\alpha_S(\mu^2)}{d\ln\mu^2} = \beta(\alpha_S(\mu^2)) = -\sum_{n=0}^{\infty}\beta_n\left(\frac{\alpha_S}{\pi}\right)^{n+1} \quad . \tag{15}$$

Note that the $g_N^{(3)}$ function is singular in $\lambda = 1$. These singularities, which are related (when $b \sim 1/\Lambda_{\mathrm{QCD}}$) to the divergent behavior of the perturbative running coupling α_S/π near the Landau pole, signal the onset of non-perturbative phenomena at very large values of b or, equivalently, in the region of very small transverse momenta.This type of singularities is a common feature of all-order resummation formulae of soft-gluon contributions. Within a perturbative framework, these singularities have to be regularized.

2.1.2 The finite component at NNLO

The finite component $d\hat{\sigma}^{(\mathrm{fin.})}_{Fab}$ of the transverse-momentum cross section is computed at a given perturbative order in α_S. As discussed in sec. 2.1 and 2.1.1 , the finite component $d\hat{\sigma}^{(\mathrm{fin.})}_{Fab}$ does not contain any perturbative contributions proportional to $\delta(p_T^2)$ (these contributions and all the logarithmically-enhanced terms at small-p_T are included in $d\hat{\sigma}^{(\mathrm{res.})}_{Fab}$). At a given order it is just evaluated by inverting Eq. 7 as follows

$$\left[\frac{d\hat{\sigma}^{(\mathrm{res.})}_{Fab}}{dp_T^2}\right]_{(\mathrm{order})} = \left[\frac{d\hat{\sigma}_{Fab}}{dp_T^2}\right]_{(\mathrm{order})} - \left[\frac{d\hat{\sigma}^{(\mathrm{fin.})}_{Fab}}{dp_T^2}\right]_{(\mathrm{f.o.})}, \tag{16}$$

where "order" indicates a given order in perturbation theory. The fixed-order truncation of the resummed part is obtained by perturbatively expanding the resummed component $d\hat{\sigma}^{(\mathrm{res.})}$ in Eq. 9. The contributions $[d\hat{\sigma}]_{(\mathrm{f.o.})}$ on the right-hand side of Eq 16 are obtained by computing the perturbative expansion for the partonic cross section at a given order. To explain this purpose we define

$$\begin{aligned}
&\mathcal{W}^F_{ab}\left(z,\tilde{L},\frac{m_V^2}{\mu_R^2},\frac{m_V^2}{\mu_F^2},\frac{m_V^2}{Q^2}\right) = \sum_c \sigma^{(0)}_{c\bar{c},F}(\alpha_S,m_V)\left\{\delta_{ca}\delta_{\bar{c}b}(1-z)\right\} + \\
&+\sigma^{(0)}_{c\bar{c},F}(\alpha_S,m_V)\sum_{n=1}^{\infty}\left\{\left(\frac{\alpha_S}{\pi}\right)^n\left[\tilde{\Sigma}^{F(n)}_{c\bar{c}\to ab}\left(z,\tilde{L},\frac{m_V^2}{\mu_R^2},\frac{m_V^2}{\mu_F^2},\frac{m_V^2}{Q^2}\right)\right]\right\} + \\
&+\sigma^{(0)}_{c\bar{c},F}(\alpha_S,m_V)\left\{\left(\frac{\alpha_S}{\pi}\right)^n\left[\mathcal{H}^{F(n)}_{c\bar{c}\to ab}\left(z,\tilde{L},\frac{m_V^2}{\mu_R^2},\frac{m_V^2}{\mu_F^2},\frac{m_V^2}{Q^2}\right)\right]\right\}
\end{aligned} \tag{17}$$

where $z = m_V^2/\hat{s}$, $\sigma^{(0)}(\alpha_S,m_V) = \alpha^{p_{cF}}\sigma^{(\mathrm{LO})}(m_V)$ and, in general, the power p_{cF} depends on the lowest-order partonic subprocess $c\bar{c}\to F$. $\mathcal{W}^F_{ab}$ is the resummed cross section on the right-hand side of Eq. 9. Note, however, that Eq. 17 depends on the resummation scale Q^2. The dependence on the resummation scale has been introduced above through the replacement in Eq 7. The perturbative coefficient $\tilde{\Sigma}^{F(n)}$ is a polynomial of $2n$ degree. At the NNLO we get the following result

$$\begin{aligned}
&\left(\frac{\alpha_S}{\pi}\right)^n\frac{m_V^2}{\hat{s}}\sum_c \sigma^{(0)}_{c\bar{c},F}(\alpha_S,m_V)\mathcal{H}^{F(2)}_{c\bar{c}\to ab}\left(z,\tilde{L},\frac{m_V^2}{\mu_R^2},\frac{m_V^2}{\mu_F^2},\frac{m_V^2}{Q^2}\right) \\
&= \left[\hat{\sigma}^{\mathrm{tot}}_{Fab}\right]_{\mathrm{NNLO}} - \left[\hat{\sigma}^{\mathrm{tot}}_{Fab}\right]_{\mathrm{NLO}} - \int_0^{\infty} dp_T^2\left[\frac{d\hat{\sigma}^{(\mathrm{fin.})}_{Fab}}{dp_T^2}\right]_{\mathrm{NLO}} - \left[\frac{d\hat{\sigma}^{(\mathrm{fin.})}_{Fab}}{dp_T^2}\right]_{\mathrm{LO}}.
\end{aligned} \tag{18}$$

We will focus on Eqs. 18 and 12 for our studies.

3 DYRes and DYqT computational results

This section is devoted to numerical simulations along with comparisons of DYRes and DYqT W pT spectra. Firstly, we report a brief description of the main characteristics of the software as well as structural differences. We will continue the analysis presenting DYRes and DYqT results. Finally, we compare distributions and discuss outstanding items concerning simulations.

3.1 DYRes and DYqT p_T Distributions: differences between programs

The DYqT program computes the transverse-momentum spectrum of Drell–Yan lepton pairs with high invariant mass (M) produced via vector boson V ($V = W^{\pm}, Z - \gamma$) decay in pp or $p\overline{p}$ collisions. The DYqT calculation combines the fixed-order result at high values of p_T up to $\mathcal{O}(\alpha_S^2)$ with the resummation of the logarithmically enhanced contributions at small values of p_T ($p_T \ll M$) up to NNLL accuracy. The rapidity of the vector boson and the leptonic kinematical variables are integrated over the entire kinematical range.
The program performs the resummation of the large logarithmic contributions that appear in the region where the vector boson transverse-momentum is much smaller than the invariant mass M. The program can be used at NLL+LO and NNLL+NLO accuracy. At NLL+LO accuracy the resummed part is evaluated at NLL accuracy, and the fixed-order part is evaluated at LO (it is given by the $\mathcal{O}(\alpha_S)$ terms with 'V + 1 parton' in the final state). At NNLL+NLO accuracy the resummed part is evaluated at NNLL accuracy, and the fixed-order part is evaluated up to NLO (it includes all the terms with 'V + 1 parton' and 'V + 2 partons' up to $\mathcal{O}(\alpha_S^2)$) at NLO (V + 1 or 2 partons). At NNLL+NLO (NLL+LO) accuracy the DYqT calculation exactly recovers the total cross section at NNLO (NLO) upon integration over p_T.

The DYRes program is a Monte-Carlo-based code that uses VEGAS integration system in order to compute the total cross section of vector boson leptonic decay in pp or $p\overline{p}$ collisions at a given center-of-mass energy and perturbative order in QCD.
DYRes combines the calculation of the cross section up to NNLO with the resummation of the logarithmically-enhanced contributions at small transverse momenta up to NNLL in QCD perturbation theory. The program includes $Z - \gamma$ interference, finite-width effects and the leptonic decay of the vector boson with the corresponding spin correlations. The calculation retains the full kinematics of the vector boson and of its decay products, allowing the user to apply arbitrary cuts on the final state, and to plot the corresponding distributions in the form of bin histograms. The decay modes included are $W^{\pm} \to l^{\pm}\nu_l$ and $Z^0/\gamma \to l^+l^-$. The DYRes program computes the cross section of Drell–Yan lepton pairs with high invariant mass M ($M \gg \Lambda_{\rm QCD}$) produced, via vector boson V ($V = W^{\pm}, Z/\gamma$) decay, in hadronic collisions, performing the resummation of the large logarithmic contributions which appear when the vector boson transverse momentum p_T is much smaller than the invariant mass M ($p_T \ll M$). The calculation includes the leptonic decay of the vector boson with the corresponding spin correlations, retaining the full dependence on the final-state lepton(s) kinematics, the $Z - \gamma$ interference and the finite-width effects. We implement the leptonic decay $W^{\pm} \to l^{\pm}\nu_l$ and $Z^0/\gamma \to l^+l^-$. The resummed result is consistently matched to the fixed-order calculation valid at high-p_T up to $\mathcal{O}(\alpha_S^2)$. The fixed-order calculation is performed with the dipole formalism [21] as implemented in the MCFM program. Since the fixed-order cross section is divergent when the transverse momentum p_T of the vector boson becomes small,a suitable counter term must be subtracted to make the result finite as $p_T \to 0$. The counter term is evaluated through an appropriate modification of the DYNNLO program [22].

3.1.1 Input parameters

Boson mass parameters are reported in the following table

Parameter	Value (GeV)
M_W	80.399
Γ_W	2.085
M_Z	91.1876
Γ_Z	2.4952

The Fermi constant is set to $G_F = 1.16637 \times 10^{-5}\text{GeV}^{-2}$ and the following CKM matrix elements are used

$$\begin{bmatrix} V_{ud} & V_{us} & V_{ub} \\ V_{cd} & V_{cs} & V_{cb} \\ V_{td} & V_{ts} & V_{tb} \end{bmatrix} = \begin{bmatrix} 0.97427 & 0.22536 & 0.00355 \\ 0.22522 & 0.97343 & 0.0414 \\ 0.00867 & 0.0404 & 0.999146 \end{bmatrix}$$

Each EW parameter is taken from the PDG 2014.The EW couplings of the W and Z bosons to quarks and leptons are treated at the tree level, so that the above parameters are sufficient to fully specify the EW content of the calculation.

Before compiling the `DYRes` program, the user can choose to apply cuts on the leptonic final-state. This is done through the `cuts`-subroutine.The default version of this subroutine contains some selection cuts that are typically used in the experimental analysis. Since the resummation procedure is necessarily inclusive over the QCD radiation recoiling against the vector boson, cuts on jets or isolation cuts on final state leptons can not be implemented.

3.1.2 Simulations for the Tevatron: `DYqT` results

As discussed in the Introduction, $p\bar{p}$ collisions provide a precise strategy to make measurement of M_W. To pursue this, an accurate study for W and Z p_T spactra is needed. For the rest of this section we will focus on this topic in order to make clear the advantages of NLO+NNLL calculations in QCD compared with LO+NLL.

In order to produce p_T spectra, a set of Parton Distribution Functions (PDFs) has to be chosen. The results we expose refer to `MSTW2008`, `MSTW2004`, `NNPDF3.0` and `NNPDF2.3`[2]. Since simulations can be performed at LO+NLL as well as NLO+NNLL, it is necessary to maintain the same perturbative order for PDFs set in order not to neglect/add information throughout the computation. Thus, we will use PDFs both at NLO and NNLO depending on the perturbative order used in software.

The first set of results we present refers to the following input setting

Parameter	Value (GeV)
M_W	80.399
Γ_W	2.085
M_Z	91.1876
Γ_Z	2.4952
PDF set	`MSTW2008`
μ_R	$M_b/4, M_b/2, M_b$
μ_F	$M_b/4, M_b/2, M_b$
Q	M_b

[2]In this work we refer to the following specific PDFs sets: MSTW2008nlo68cl, MRST2004nlo, NNPDF30nloAs0118, NNPDF23nloAs0118; so as for nnlo

A factor of 2 in scaling μ_R, μ_F is used to estimate theoretical uncertainties on p_T spectra.

The distributions for the Z boson obtained according to the setting above are the following

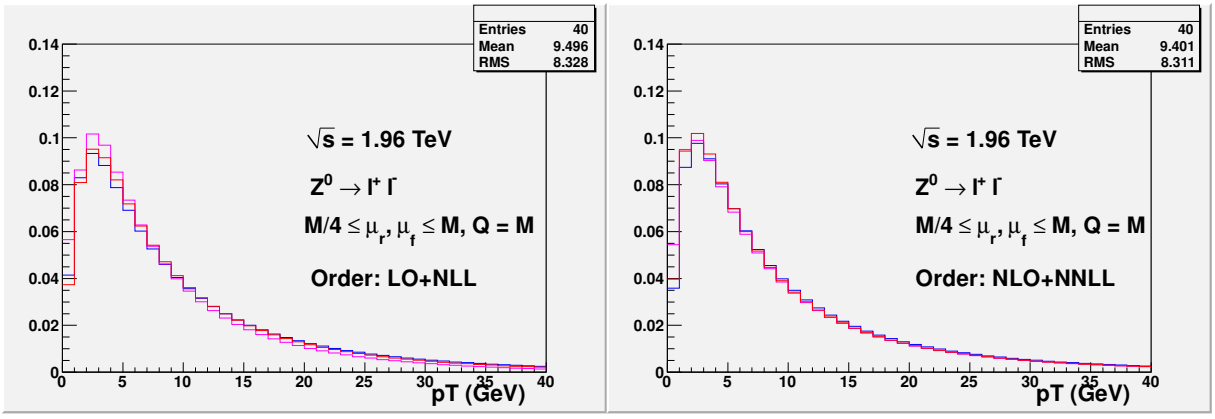

Figure 1: *Left Panel*: Transverse-momentum spectrum for Z boson production at LO+NLL. *Right Panel*: Transverse-momentum spectrum for Z boson production at NLO+NNLL. The ■ refers to un-scaled μ_R and μ_F, the ■ to $\mu_R, \mu_F = M_b/4$ and the ■ to $\mu_R, \mu_F = M_b/2$. In each run the resummation scale Q is set to $Q = M_b$.

As shown in the *Left Panel*, the scaling of μ_R, μ_F affects the computation by producing a band for each bin. In this way p_T spectra are close in the range $[10, 40]$ GeV and present an overlap at low-p_T (≤ 5 GeV). At a higher perturbative order we get data less affected by scaling, as reported in the *Right Panel*. This is due to low-energy jets production that affects more the computation as the perturbative order increases. This effect is more visible varying the auxiliary scale Q as well.

For the W boson - with the same setting - we obtain the following distributions

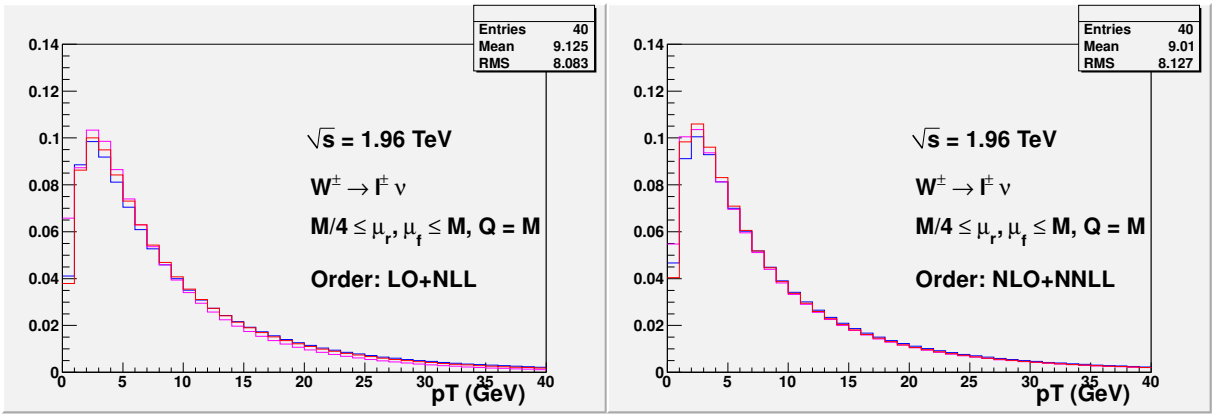

Figure 2: *Left Panel*: Transverse-momentum spectrum for W boson production at LO+NLL. *Right Panel*: Transverse-momentum spectrum for W boson production at NLO+NNLL. The ■ refers to un-scaled μ_R and μ_F, the ■ to $\mu_R, \mu_F = M_b/4$ and the ■ to $\mu_R, \mu_F = M_b/2$. In each run the resummation scale Q is set to $Q = M_b$.

At a lower perturbative order, the W boson distributions are scaled as Z distributions. More quantitatively, in the peaks region the spread is about 0.5%. Along the intermediate as well as high region of p_T the NLO+NNLL produces thinner band for both bosons.

In order to study the relation between W and Z p_T spectra, we compute the ratio of distributions p_T^W/p_T^Z at the same perturbative order. The plots below refer to the current initial setting for `DYqT`.

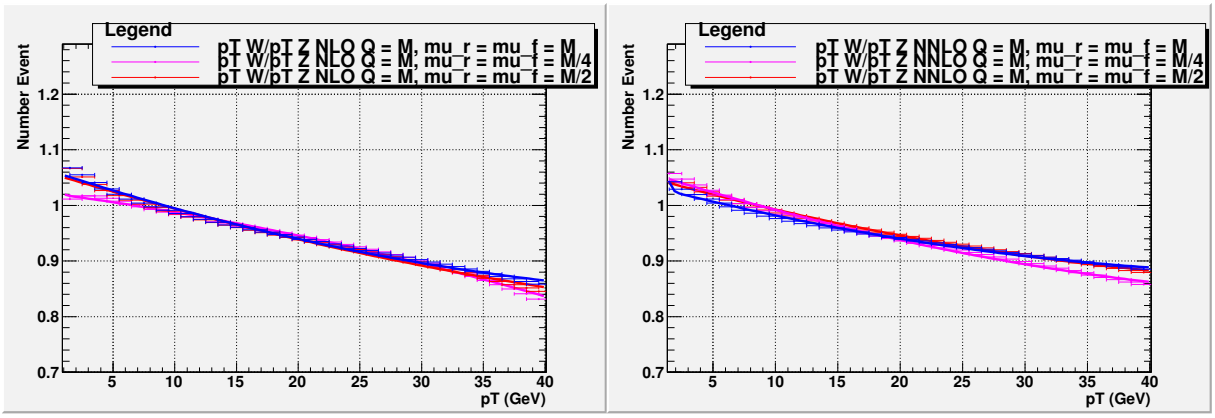

Figure 3: *Left Panel*: p_T^W/p_T^Z ratio distribution at LO+NLL. *Right Panel*: p_T^W/p_T^Z ratio distribution at NLO+NNLL. The ■ refers to un-scaled μ_R and μ_F, the ■ to $\mu_R, \mu_F = M_b/4$ and the ■ to $\mu_R, \mu_F = M_b/2$. In each run the resummation scale Q is set to $Q = M_b$. At a higher perturbative order in QCD the band is thinner than LO+NLL.

Note that keeping the resummation scale Q constant, even if p_T spectra are subjected by scaling, the ratio distributions present almost a total overlap along the p_T range investigated. Notice that at LO+NLL the spread at low-p_T is about 5%, it decreases to less than 1% in intermediate region and increases up to 3% in the high-p_T region. The NLO+NNLL perturbative order presents slightly different trends. Distributions look very similar at low-p_T and have much more agreement along the whole range of computation up to 40 GeV where the spread is roughly 2%.

In order to better understand the impact of theoretical scaling, we perform a different run of `DYqT` according to the following table of parameters [3]

Parameter	Value (GeV)
μ_R	$M_b/4, M_b/2, M_b$
μ_F	$M_b/4, M_b/2, M_b$
Q	$M_b/4, M_b/2, M_b$

The difference from the first run is stated by a variation of Q. The following are the distributions obtained for Z boson production

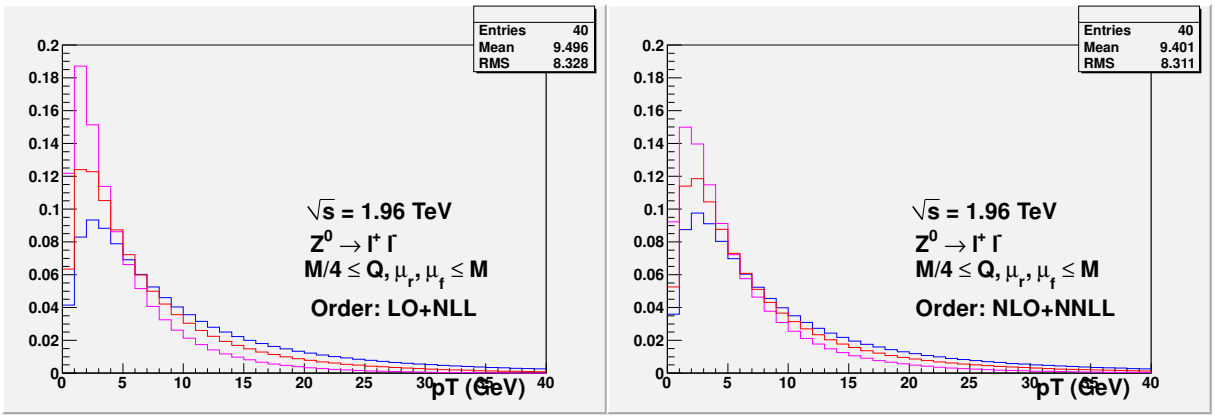

Figure 4: *Left Panel*: Transverse-momentum spectrum for Z boson production at LO+NLL. *Right Panel*: Transverse-momentum spectrum for W boson production at NLO+NNLL. The ■ refers to un-scaled μ_R and μ_F, the ■ to $\mu_R, \mu_F = M_b/4$ and the ■ to $\mu_R, \mu_F = M_b/2$. In each run the resummation scale Q takes the same value of other scales.

In the case of W boson production we have the following results

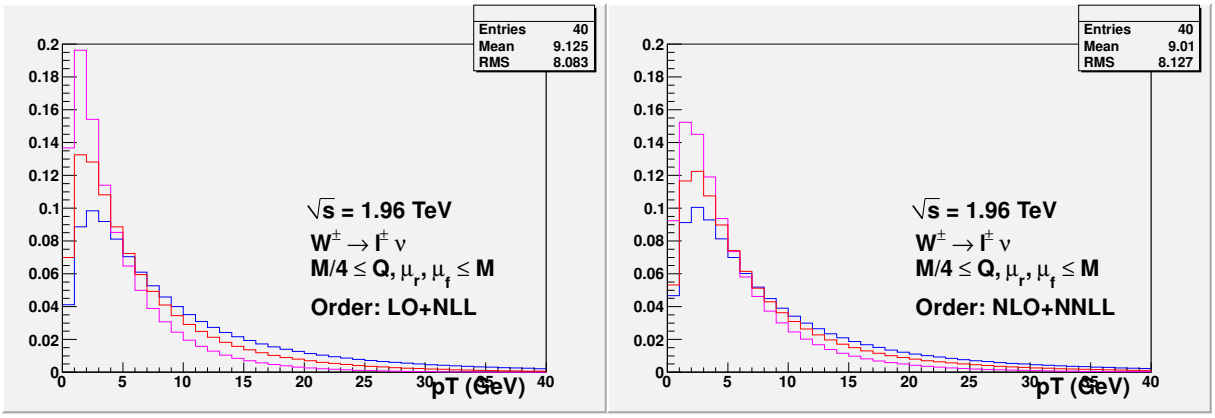

Figure 5: *Left Panel*: Transverse-momentum spectrum for W boson production at LO+NLL. *Right Panel*: Transverse-momentum spectrum for W boson production at NLO+NNLL. The ■ refers to un-scaled μ_R and μ_F, the ■ to $\mu_R, \mu_F = M_b/4$ and the ■ to $\mu_R, \mu_F = M_b/2$. In each run the resummation scale Q takes the same value of others scales.

[3] Mass parameters are the same as the first table.

As sketched by distributions, the resummation scaling affects seriously the computation of p_T distributions for both bosons. At LO+NLL the difference near peaks is 45% and decreases to about 20% at NLO+NNLL. This result is due to the particular form of the resummation factor $g_N^{(3)}$ in the case in which $Q = \mu_R = \mu_F$. The NNLL correction takes the following form

$$g_N^{(3)}\left(\alpha_S L, \frac{m_V^2}{\mu_R^2}, \frac{m_V^2}{Q^2}\right) = -\frac{A^{(3)}}{2\beta_0^2}\frac{\lambda^2}{(1-\lambda)^2} - \frac{\overline{B}_N^{(2)}}{\beta_0}\frac{\lambda}{1-\lambda} + \frac{A^{(2)}\beta_1}{\beta_0}\left(\frac{\lambda}{2}\frac{(3\lambda-2)}{2(1-\lambda)^2} - \frac{(1-2\lambda)\ln(1-\lambda))}{(1-\lambda)^2}\right) + \\ + \frac{\overline{B}_N^{(1)}\beta_1}{\beta_0^2}\left(\frac{\lambda}{1-\lambda} + \frac{\ln(1-\lambda)}{1-\lambda}\right) \\ + A^{(1)}\left(\frac{\beta_1^2}{2\beta_0^2}\frac{1-2\lambda}{(1-\lambda)^2}\ln^2(1-\lambda) + \ln(1-\lambda)\left[\frac{\beta_0\beta_2-\beta_1^2}{\beta_0^4} + \frac{\beta_1^2}{\beta_0^4(1-\lambda)} + \left(\beta_0\beta_2(2-3\lambda)+\beta_1^2\lambda\right)\right]\right) \tag{19}$$

where - in this case - the coefficients $\overline{B}_N^{(n)} = B_N^{(n)}$.

Let us consider the ratio distributions p_T^W/p_T^Z

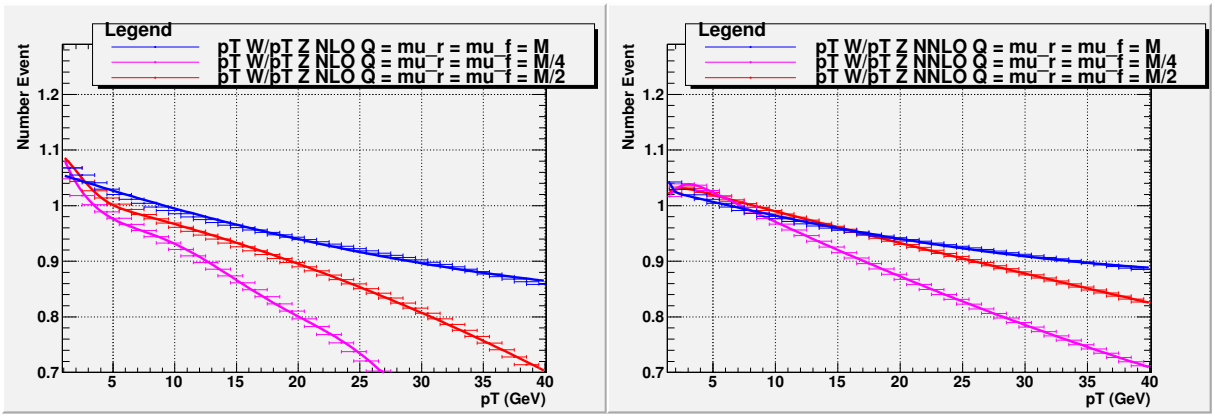

Figure 6: *Left Panel*: p_T^W/p_T^Z ratio distribution at LO+NLL. *Right Panel*: p_T^W/p_T^Z ratio distribution at NLO+NNLL.The ■ refers to un-scaled μ_R and μ_F, the ■ to $\mu_R, \mu_F = M_b/4$ and the ■ to $\mu_R, \mu_F = M_b/2$. In each run the resummation scale Q is set to $Q = M_b$.

Notice that, despite an increasing spread as p_T increases, at low-p_T there is an agreement at both perturbative orders. In this input setting, different scaling of Q produce drastic differences in ratio distributions as p_T increases. In particular, at LO+NLL the spread is much higher than NLO+NNLL. Ratio distributions depend on the resummation scaling. It is useful to understand in which range of p_T the resummation scale has a strong impact on theoretical predictions. A complete analysis of this aspect can be pursued by keeping the scales μ_R and μ_F fixed ($= M_b$) and varying $Q = M_b, M_b/2, M_b/4$. In this way we expect to figure out which values of Q affect more the production of W and Z.

Thus, the following plots refer to the setting-table

Parameter	Value (GeV)
μ_R	M_b
μ_F	M_b
Q	$M_b/4, M_b/2, M_b$

For the Z boson spectra we obtain the following results

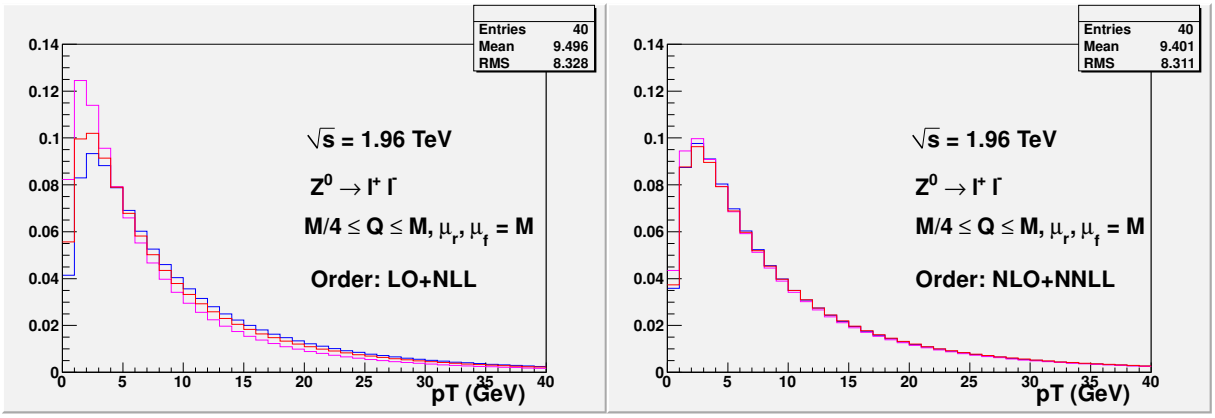

Figure 7: *Left Panel*: Transverse-momentum spectrum for Z boson production at LO+NLL. *Right Panel*: Transverse-momentum spectrum for W boson production at NLO+NNLL. The ■ refers to un-scaled μ_R, μ_F, Q, the ■ to $Q = M_b/4$ and the ■ to $Q = M_b/2$. In each run the resummation scale μ_R, μ_F take the same value of boson masses.

Results for the W are

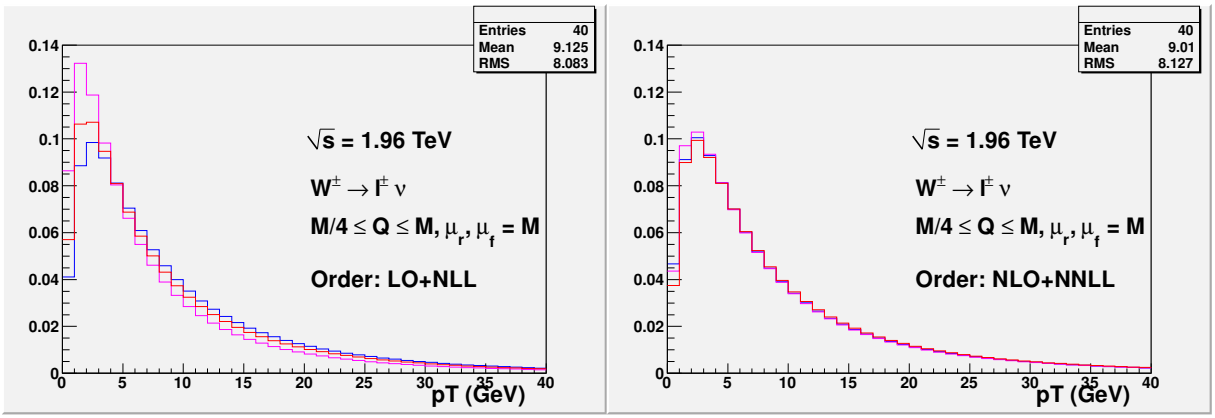

Figure 8: *Left Panel*: Transverse-momentum spectrum for W boson production at LO+NLL. *Right Panel*: Transverse-momentum spectrum for W boson production at NLO+NNLL. The ■ refers to un-scaled μ_R, μ_F, Q, the ■ to $Q = M_b/4$ and the ■ to $Q = M_b/2$. In each run the resummation scale μ_R, μ_F take the same value of boson masses.

At LO+NLL the spread in the peak region is about 20% and decreases drastically at the highest perturbative order to roughly 1%.

Ratio distributions

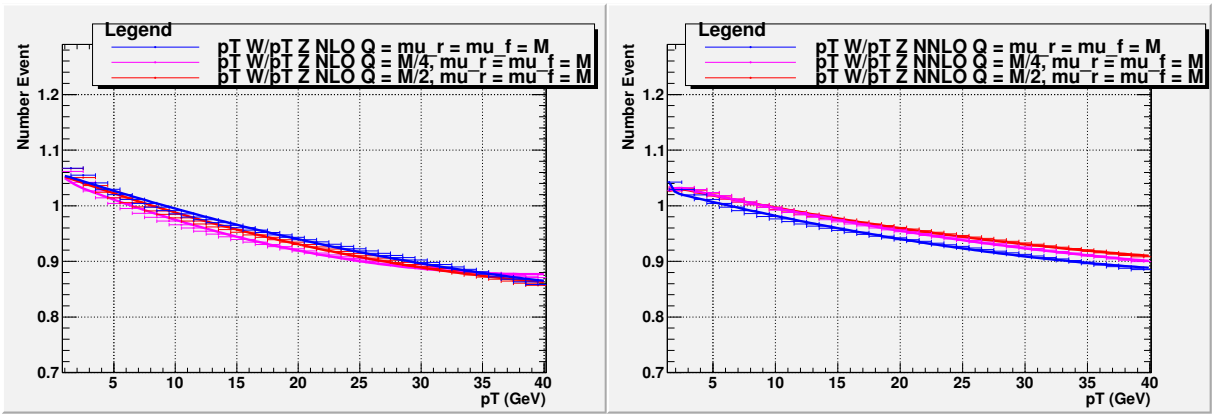

Figure 9: *Left Panel*: p_T^W/p_T^Z ratio distribution at LO+NLL. *Right Panel*: p_T^W/p_T^Z ratio distribution at NLO+NNLL. T the ■ refers to un-scaled μ_R, μ_F, Q, the ■ to $Q = M_b/4$ and the ■ to $Q = M_b/2$. In each run the resummation scale μ_R, μ_F take the same value of boson masses.

Ratio distributions present the same trends along the whole range of p_T investigated. Notice that, despite the scaling of auxiliary scales μ_R, μ_F, Q gives us a precise method for studying theoretical errors, the renormalization scale is not a theoretical assumption and should be chosen as close as possible to the mass of boson. Thus, ratio distributions do not depend from the scaling of μ_R, μ_F, as we expected. In fact μ_R, μ_F do not have to cause any dependence in physical results. Thus, the spread at low-p_T might be due to the PDF set used for computation.To analyze this topic in more detail we use `MSTW2004`, `NNPDF3.0` and `NNPDF2.3` plus scaling μ_R, μ_F.

The following results refer to the following setting-table

Parameter	Value (GeV)
μ_R	$M_b/4, M_b/2, M_b$
μ_F	$M_b/4, M_b/2, M_b$
Q	M_b
PDF set	`MSTW2004`

Z boson distributions

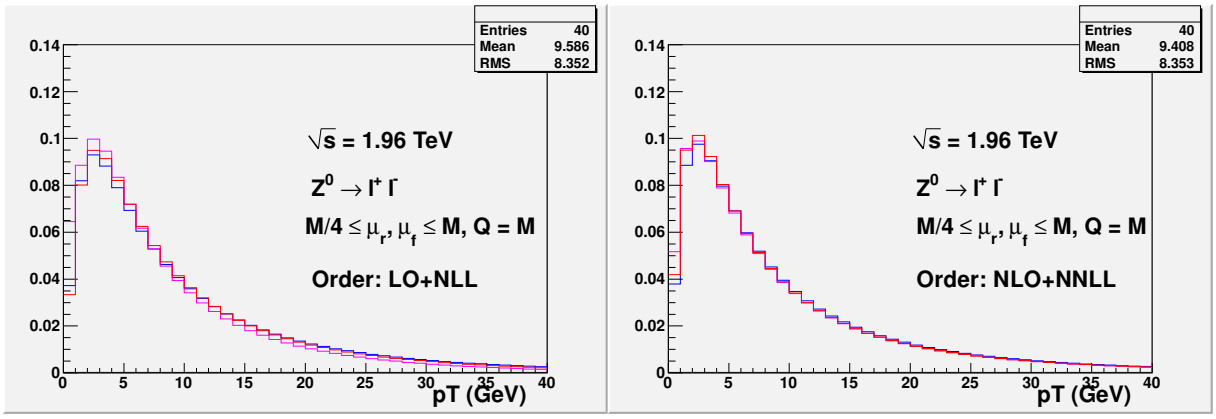

Figure 10: *Left Panel*: *Left Panel*: Transverse-momentum spectrum for Z boson production at LO+NLL. *Right Panel*: Transverse-momentum spectrum for Z boson production at NLO+NNLL. The ■ refers to un-scaled μ_R and μ_F, the ■ to $\mu_R, \mu_F = M_b/4$ and the ■ to $\mu_R, \mu_F = M_b/2$. In each run the resummation scale Q is set to $Q = M_b$.

W boson distributions

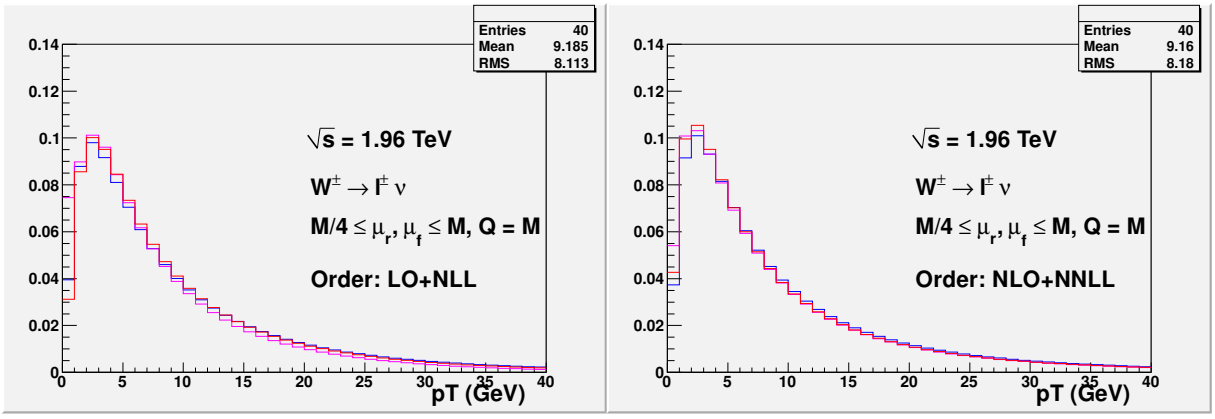

Figure 11: *Left Panel*: Transverse-momentum spectrum for W boson production at LO+NLL. *Right Panel*: Transverse-momentum spectrum for W boson production at NLO+NNLL. The ■ refers to un-scaled μ_R and μ_F, the ■ to $\mu_R, \mu_F = M_b/4$ and the ■ to $\mu_R, \mu_F = M_b/2$. In each run the resummation scale Q is set to $Q = M_b$.

`MSTW2004` provides distributions less affected by the scaling of μ_R, μ_F. Notice that the W boson is slightly less affected by scaling, providing less than 1% spread near peaks, whereas the Z spreads are next to 1%.

Ratio distributions

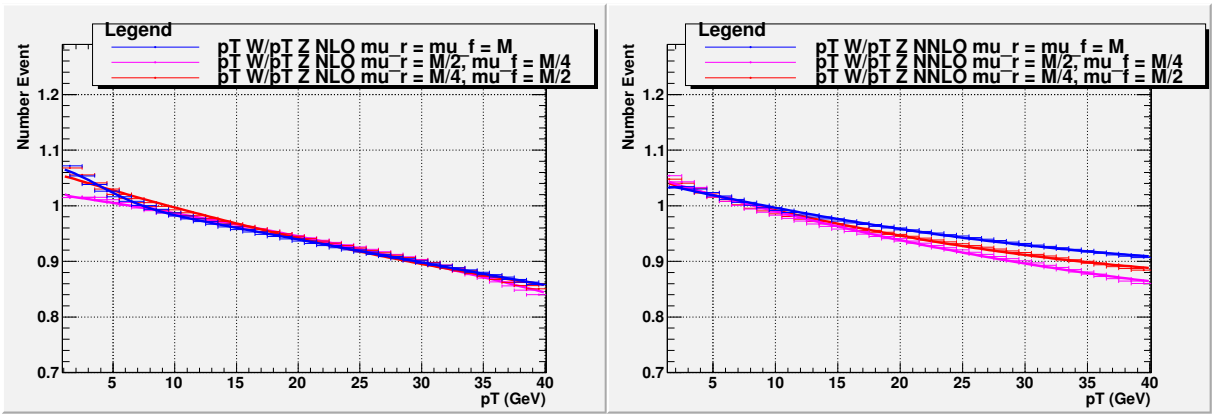

Figure 12: *Left Panel*: p_T^W/p_T^Z ratio distribution at LO+NLL. *Right Panel*: p_T^W/p_T^Z ratio distribution at NLO+NNLL. The ■ refers to un-scaled μ_R, μ_F, Q, the ■ to $Q = M_b/4$ and the ■ to $Q = M_b/2$. In each run the resummation scale μ_R, μ_F take the same value of boson masses.

Notice that `MSTW2004` produces an increasing spread as p_T increases in the intermediate and high-p_T regions. This is a remarkable difference compared with `MSTW2008` set. At LO+NLL in low-p_T region the spread is 3%, decreases to about 1% in the intermediate region to increase slightly up to 2% at 40 GeV. The NLO+NNLL has 1% spread at low-p_T, 3% in the intermediate region and an increasing trend up to 5% near 40 GeV.

The last PDF set we use is `NNPDF3.0`. The following results refer to the following setting-table

Parameter	Value (GeV)
μ_R	$M_b/4, M_b/2, M_b$
μ_F	$M_b/4, M_b/2, M_b$
Q	M_b
PDF set	`NNPDF3.0`

Z boson production

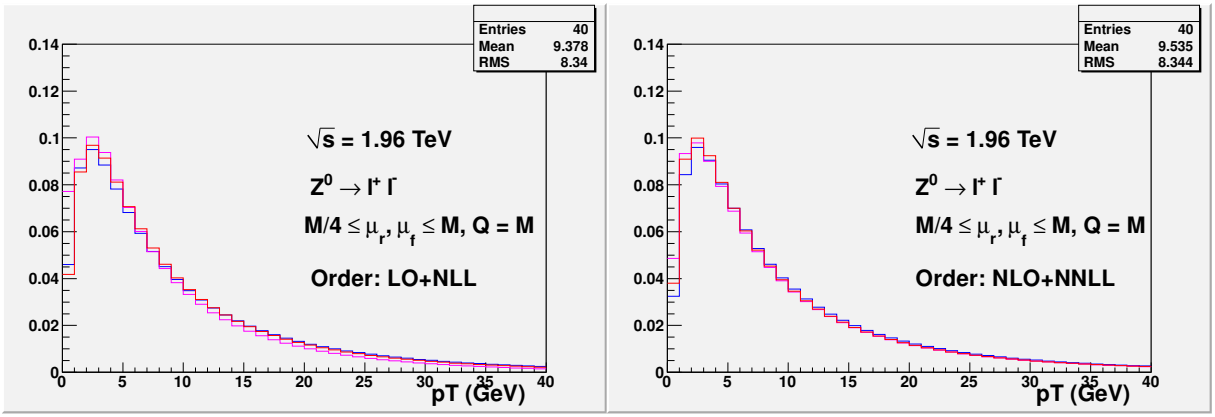

Figure 13: *Left Panel*: *Left Panel*: Transverse-momentum spectrum for Z boson production at LO+NLL. *Right Panel*: Transverse-momentum spectrum for Z boson production at NLO+NNLL. The ■ refers to unscaled μ_R and μ_F, the ■ to $\mu_R, \mu_F = M_b/4$ and the ■ to $\mu_R, \mu_F = M_b/2$. In each run the resummation scale Q is set to $Q = M_b$.

W boson production

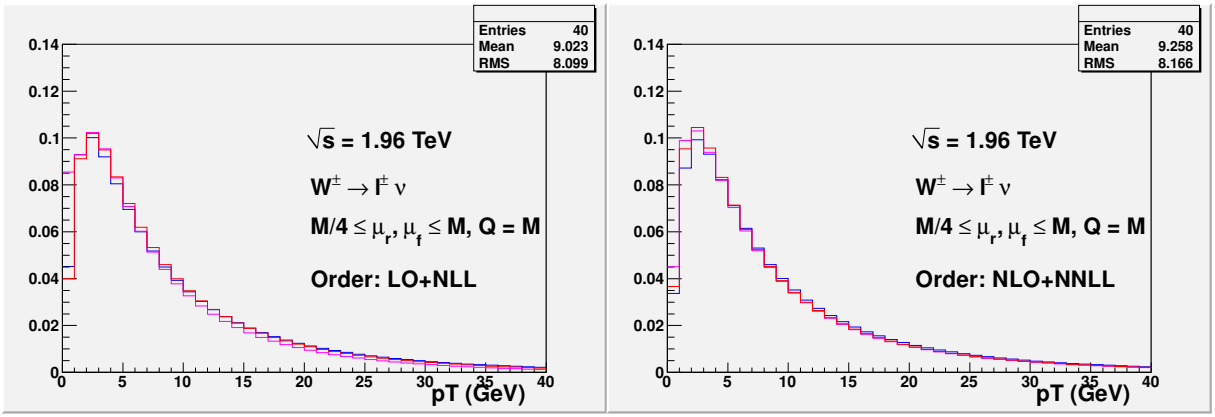

Figure 14: *Left Panel*: *Left Panel*: Transverse-momentum spectrum for W boson production at LO+NLL. *Right Panel*: Transverse-momentum spectrum for W boson production at NLO+NNLL.The ■ refers to unscaled μ_R and μ_F, the ■ to $\mu_R, \mu_F = M_b/4$ and the ■ to $\mu_R, \mu_F = M_b/2$. In each run the resummation scale Q is set to $Q = M_b$.

Ratio distributions

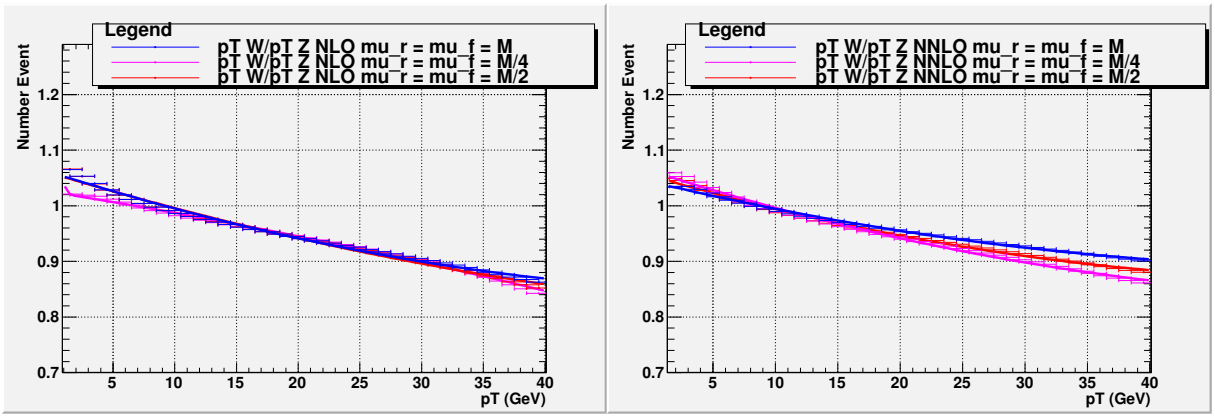

Figure 15: *Left Panel*: p_T^W/p_T^Z ratio distribution at LO+NLL. *Right Panel*: p_T^W/p_T^Z ratio distribution at NLO+NNLL.The ■ refers to un-scaled μ_R, μ_F, Q, the ■ to $Q = M_b/4$ and the ■ to $Q = M_b/2$. In each run the resummation scale μ_R, μ_F take the same value of boson masses.

At LO+NLL a similar trend is obtained at low-p_T along with the increasing spread in intermediate and high-p_T region at NLO+NNLL. Notice that `NNPDF3.0` gives thinner bands. To be consistent, the last PDFs set we use is `NNPDF2.3`, the following are the results obtained with the same type of scaling.

Z boson production

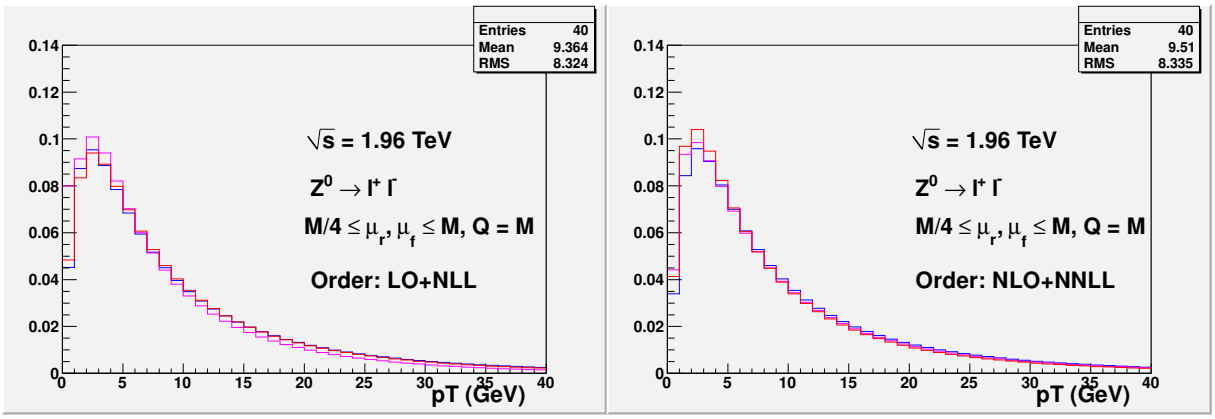

Figure 16: *Left Panel*: *Left Panel*: Transverse-momentum spectrum for Z boson production at LO+NLL. *Right Panel*: Transverse-momentum spectrum for Z boson production at NLO+NNLL. The ■ refers to un-scaled μ_R and μ_F, the ■ to $\mu_R, \mu_F = M_b/4$ and the ■ to $\mu_R, \mu_F = M_b/2$. In each run the resummation scale Q is set to $Q = M_b$.

W boson production

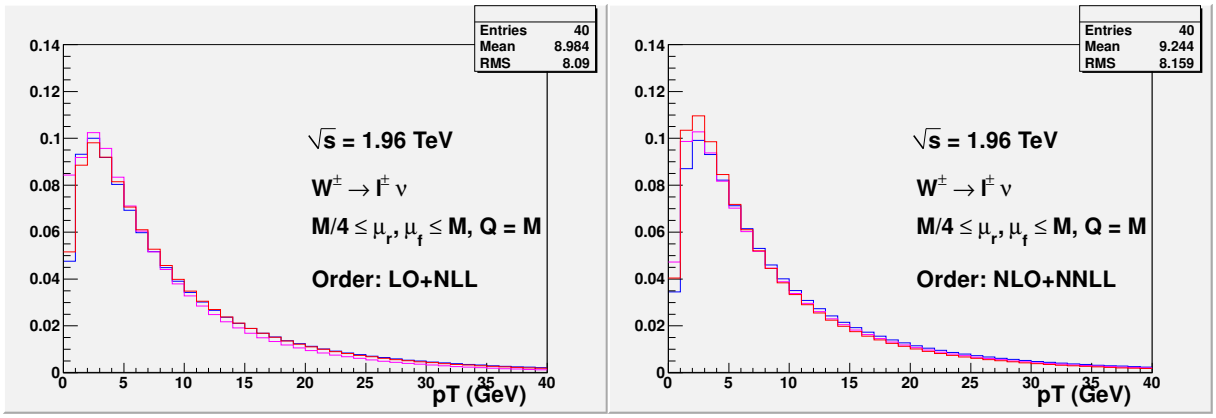

Figure 17: *Left Panel*: *Left Panel*: Transverse-momentum spectrum for Z boson production at LO+NLL. *Right Panel*: Transverse-momentum spectrum for Z boson production at NLO+NNLL. The ■ refers to un-scaled μ_R and μ_F, the ■ to $\mu_R, \mu_F = M_b/4$ and the ■ to $\mu_R, \mu_F = M_b/2$. In each run the resummation scale Q is set to $Q = M_b$.

Ratio distributions

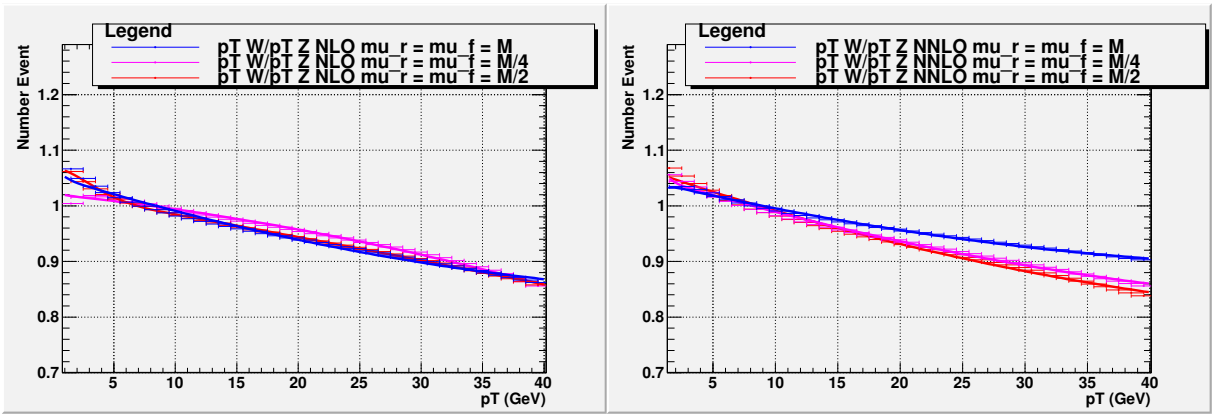

Figure 18: *Left Panel*: p_T^W/p_T^Z ratio distribution at LO+NLL. *Right Panel*: p_T^W/p_T^Z ratio distribution at NLO+NNLL.The ■ refers to un-scaled μ_R and μ_F, the ■ to $\mu_R, \mu_F = M_b/4$ and the ■ to $\mu_R, \mu_F = M_b/2$. In each run the resummation scale Q is set to $Q = M_b$.

In the low-p_T region the LO+NLL band is about 5%, decreases to about 2% near 20 GeV where `NNPDF2.3` presents a slight overestimation ($\approx 1\%$) from other sets and is reduced to 1% around 40 GeV. The NLO+NNLL band has the following trend: 1% at low-p_T, 2% near 20 GeV and 6% next to 40 GeV. Notice that as p_T approaches to 40 GeV the scaled distributions at NLO+NNLL become closer forming a sub-band of roughly 2%. As final discussion we present a summary plot including ratios at different perturbative orders in QCD using the PDFs set we have as far.

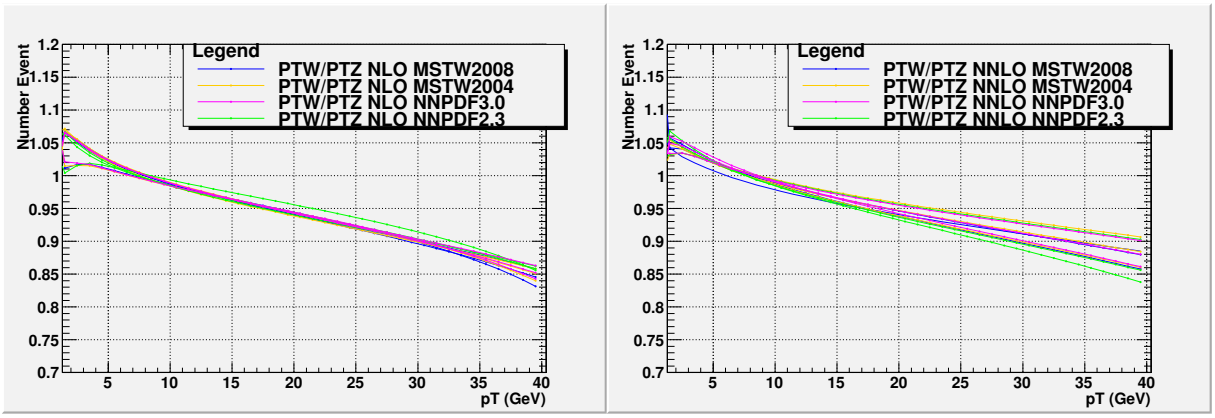

Figure 19: *Left Panel*: p_T^W/p_T^Z ratio distribution at LO+NLL. *Right Panel*: p_T^W/p_T^Z ratio distribution at NLO+NNLL.The ■ refers to `MSTW2008`, the ■ to `NNPDF3.0`, the ■ to `NNPDF2.3` and the ■ to `MSTW2004`.

At LO+NLL (right panel) distributions present a similar trend in each range of p_T. At low-p_T the band is roughly 5% and ratios do not present shift when changing PDF set. The spread is reduced to about 1% at intermediate-p_T and increases up to 3% near 40 GeV. A slightly divergent trend is observed at NLO+NNLL order. At low-p_T the spread for each PDF set is shrunk to 2%, in the intermediate-p_T region increases up to 3% reaching 6% at 40 GeV. Notice that `MSTW2008` slightly underestimates data at low-p_T. Notice that `NNPDF3.0` present a thinner band at NLO+NNLL, especially in the low-p_T region.

A different way to perform theoretical scaling is to change each auxiliary scale with no dependence on each others. Notice that the results we have discussed as far combine at least 2 out of 3 auxiliary scales equal to each others. What we report now refer to the following setting-table. We use `MSTW2004`, `MSTW2008`, `NNPDF2.3` and `NNPDF3.0` so as to compare consistent PDFs sets. Thus, the results below refer to the following setting-table

Parameter	**Value (GeV)**
μ_R	$M_b/4, M_b/2, M_b$
μ_F	$M_b/2, M_b/4, M_b$
Q	M_b

In this way we consider non dependent scales for each run, providing a different method to perform the scaling that can be compared with the one discussed as far. The aim of this study is to obtain two ways to estimate theoretical uncertainties on ratio distributions so as to use both scaling for an accurate discussion concerning the impact of theoretical errors on M_W measurement.

The analysis pursued in this case is strictly similar to the previous type of scaling. For this reason, we limit the discussion to a comparison between ratio distributions. The following are the results obtained using the same PDFs sets as above

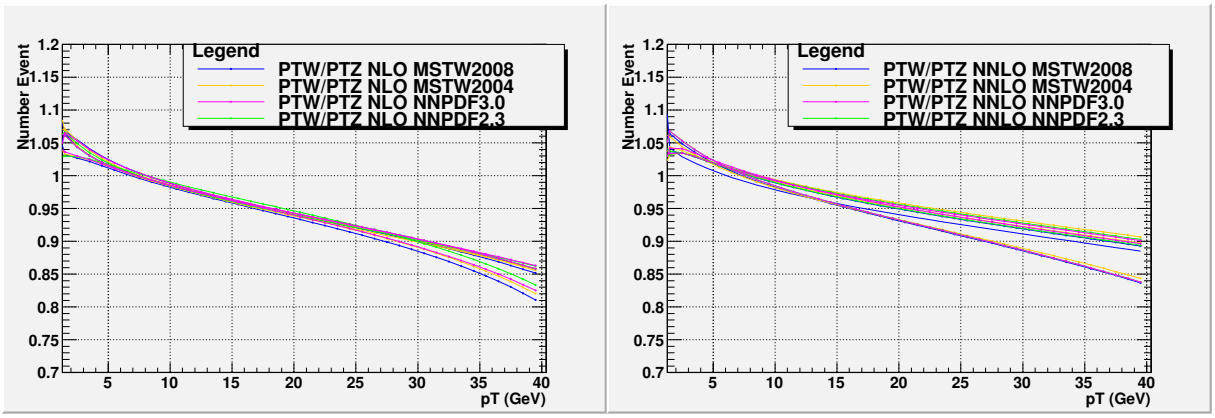

Figure 20: *Left Panel*: p_T^W/p_T^Z ratio distribution at LO+NLL. *Right Panel*: p_T^W/p_T^Z ratio distribution at NLO+NNLL.The ■ refers to `MSTW2008`, the ■ to `NNPDF3.0`, the ■ to `NNPDF2.3` and the ■ to `MSTW2004`.

Distributions present a good agreement along the range of p_T investigated. The total band is about 3% at low-p_T, 2% in the intermediate region and 5% near 40 GeV for the LO+NLL. A slightly different trend is obtained at NLO+NNLL. The spread is roughly 2% at low-p_T and increases to about 3%, reaching 6% at 40 GeV. In each case, changing PDFs set does not provide a considerable shift in the uncertainty band.

The last type of scaling we perform concerns the Non-Perturbative smearing parameter. The smearing is applied as an additional factor $\exp(-g_{NP}b^2)$ in the resummed part, where b is the impact parameter variable that is Fourier conjugated to p_T . The choice $g_{NP} = 0$ means that no smearing is applied to the perturbative result. The results we present refer to the following setting-table

Parameter	**Value (GeV)**
μ_R	$M_b/2$
μ_F	$M_b/2$
Q	$M_b/2$
g_{NP}	$(0, 1/2, 1)\text{GeV}^2$

Notice that it is not possible to compute the expected value of g_{NP} theoretically, since it has to be deduced by experimental data. The scaling reported is commonly used in literature. We will include the results for these case in the following section.

3.1.3 Simulations for the Tevatron: `DYRes` results

This section is devoted to a discussion of p_T distributions computed with `DYRes`. We remind that this program is different from `DYqT` since it allows computation both at NLO+NLL and NNLO+NNLL. We limit our discussion to the `MSTW2008` PDFs set with no theoretical scaling. We will first compare W and Z spectra, then discuss ratio distributions along with the bands we have found with `DYqT`.

The following are the p_T spectra for the Z and W boson

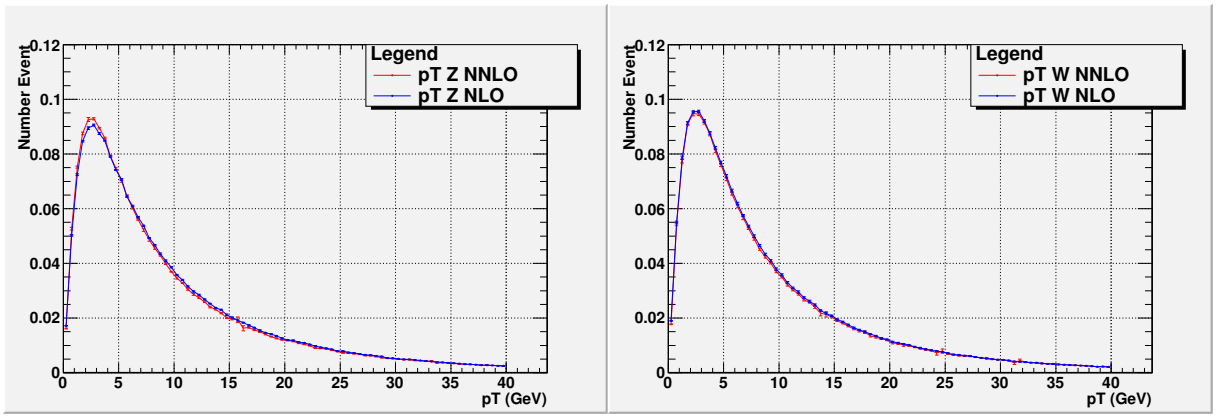

Figure 21: *Left Panel:* Z p_T spectrum at NLO+NLL and NNLLO+NNLL. *Left Panel:* W p_T spectrum at NLO+NLL and NNLLO+NNLL. Notice that Z boson distributions presents a bit larger spread ($\approx 1\%$) than the W in the peaks region.

The following plots refer to a comparison of p_T of Z and W at the same perturbative order

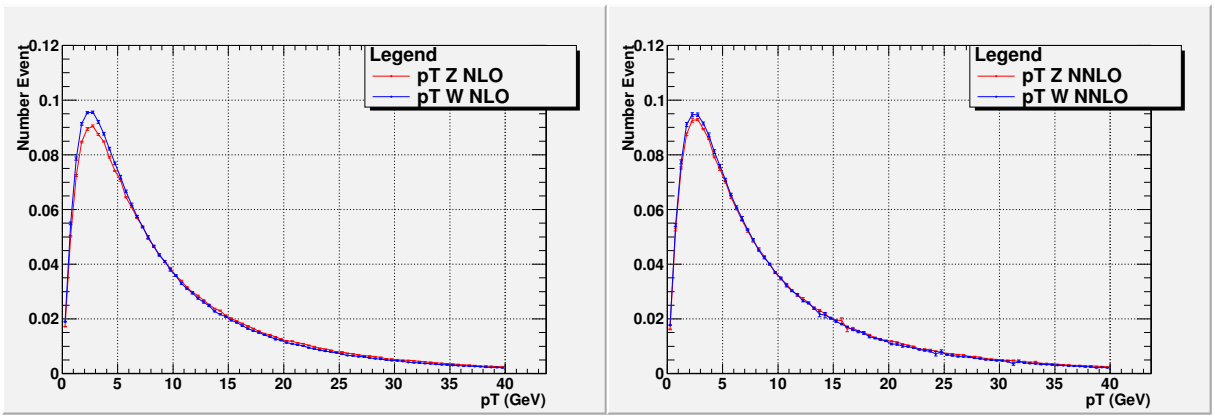

Notice that the Z boson in a bit more affected by the change from NLO+NLL to NNLO+NNLL than the W. The spread near the peak region is about 1% and is almost totally absent for the W boson. At NLO+NLL, W and Z spectra are slightly different near 2 GeV.

In order to compare DYRes data with the theoretical bands we have found, we present two summary plots comparing the two programs. We report ratio distributions below

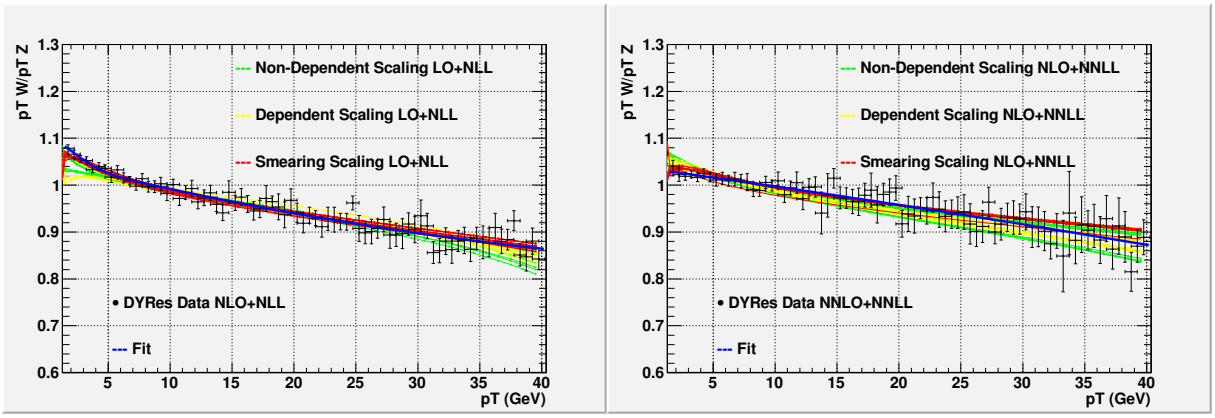

Monte-Carlo data are in good agreement with theoretical bands at each perturbative order, since a large percentage of them is included in the green as well as yellow bands, which are extremely close along the p_T range studied. Despite the difference in reachable perturbative orders of the programs, it is noticeable that data at NLO+NLL present a slight overestimation of the central value of the band of about 1.5% and at NNLO+NNLL underestimate of 1% the correspondent central value. Notice that the Non-Perturbative smearing scaling explains DYRes data trend at low-p_T providing a band of about 2%. It is remarkable that at intermediate and high-p_T the g_{NP} band ($\approx 3\%$) is thinner than other cases. We will leave this study as future progress in W p_T spectra analysis.

4 Conclusions

In this work we have presented a study of theoretical uncertainties on transverse-momentum distributions that affect the measurement of the W boson mass. Our analysis is focused on the W and Z production at the Tevatron energies as a preliminary study for a precise measurement of M_W at CDF. The specific aim we have pursued regards the impact of Renormalization, Resummation and Factorization scaling on p_T distributions. In order to provide a more general point of view, we have considered different Parton Distribution Functions sets, such as `MSTW2008`, `MSTW2004`, `NNPDF3.0` and `NNPDF2.3`. We have found that the scaling of these parameters along with the PDFs produce a $1-6\%$ theoretical error represented by a band along the p_T region investigated. Since `DYRes` data at low-p_T are subjected to over/under-estimation of theoretical uncertainties - depending on the perturbative order - the next future aim is to study the impact of non-perturbative models at low as well as intermediate and high-p_T in order to enhance uncertainties predictions in the kinematical region used for experimental measurements.

References

[1] A. Sirlin, Phys. Rev. D **22**, 971 (1980).

[2] P. Bagnaia *et al.* [UA2 Collaboration], Phys. Lett. B **129**, 130 (1983).

[3] T. Affolder *et al.* [CDF Collaboration], Phys. Rev. D **64**, 052001 (2001) [hep-ex/0007044].

[4] B. Abbott *et al.* [D0 Collaboration], Phys. Rev. D **58**, 092003 (1998) [hep-ex/9712029].

[5] T. Aaltonen *et al.* [CDF Collaboration], Phys. Rev. D **77**, 112001 (2008) [arXiv:0708.3642 [hep-ex]].

[6] V. M. Abazov *et al.* [D0 Collaboration], Phys. Rev. Lett. **103**, 141801 (2009) [arXiv:0908.0766 [hep-ex]].

[7] S. D. Drell and T. M. Yan, Phys. Rev. Lett. **25**, 316 (1970) [Phys. Rev. Lett. **25**, 902 (1970)].

[8] K. Melnikov and F. Petriello, Phys. Rev. Lett. **96**, 231803 (2006) [hep-ph/0603182].

[9] K. Melnikov and F. Petriello, Phys. Rev. D **74**, 114017 (2006) [hep-ph/0609070].

[10] R. Gavin, Y. Li, F. Petriello and S. Quackenbush, Comput. Phys. Commun. **182**, 2388 (2011) [arXiv:1011.3540 [hep-ph]].

[11] S. Catani, L. Cieri, G. Ferrera, D. de Florian and M. Grazzini, Phys. Rev. Lett. **103**, 082001 (2009) [arXiv:0903.2120 [hep-ph]].

[12] S. Catani, G. Ferrera and M. Grazzini, JHEP **1005**, 006 (2010) [arXiv:1002.3115 [hep-ph]].

[13] R. Boughezal, C. Focke, X. Liu and F. Petriello, Phys. Rev. Lett. **115**, no. 6, 062002 (2015) [arXiv:1504.02131 [hep-ph]].

[14] A. Gehrmann-De Ridder, T. Gehrmann, E. W. N. Glover, A. Huss and T. A. Morgan, arXiv:1507.02850 [hep-ph].

[15] J. C. Collins and D. E. Soper, Nucl. Phys. B **193**, 381 (1981) [Nucl. Phys. B **213**, 545 (1983)].

[16] J. C. Collins and D. E. Soper, Nucl. Phys. B **197**, 446 (1982).

[17] J. C. Collins, D. E. Soper and G. F. Sterman, Nucl. Phys. B **250**, 199 (1985).

[18] S. Catani, D. de Florian and M. Grazzini, Nucl. Phys. B **596**, 299 (2001) [hep-ph/0008184].

[19] S. Catani, D. de Florian, G. Ferrera and M. Grazzini, arXiv:1507.06937 [hep-ph].

[20] G. Bozzi, S. Catani, D. de Florian and M. Grazzini, Nucl. Phys. B **737**, 73 (2006) [hep-ph/0508068].

[21] S. Catani and M. H. Seymour, Nucl. Phys. B **485**, 291 (1997) [Nucl. Phys. B **510**, 503 (1998)] [hep-ph/9605323].

[22] S. Catani, L. Cieri, G. Ferrera, D. de Florian and M. Grazzini, Phys. Rev. Lett. **103**, 082001 (2009) [arXiv:0903.2120 [hep-ph]].